Joule

CellPress

Article

Reduced Self-Doping of Perovskites Induced by Short Annealing for Efficient Solar Modules

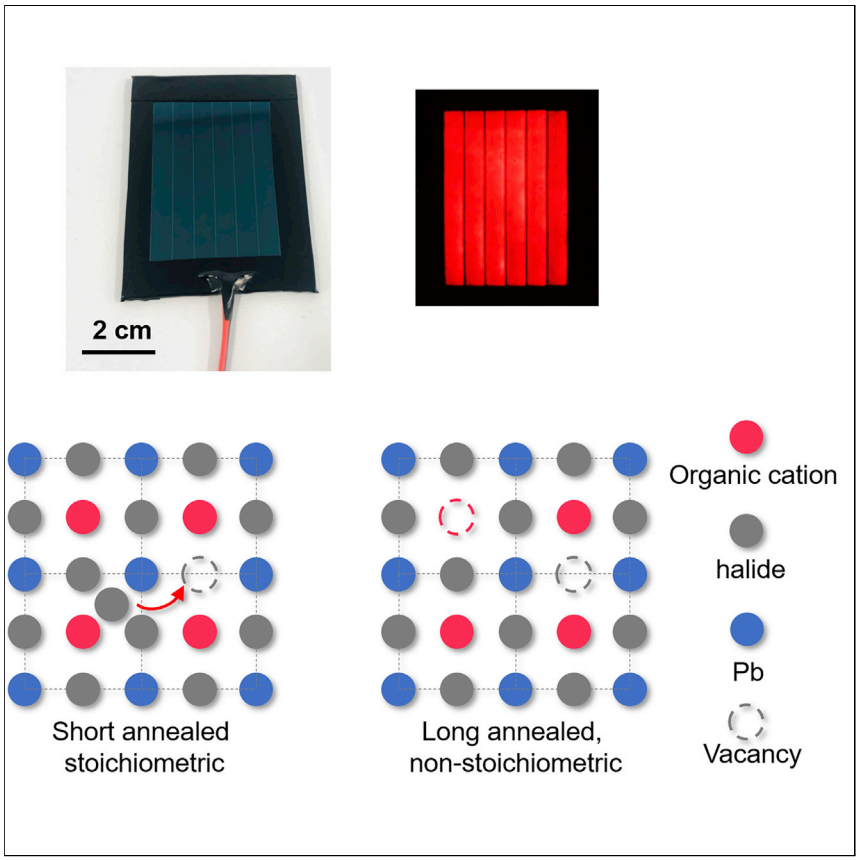

Solar panels need to be fabricated by a low-cost high-throughput process for a rapid expansion in the renewable energy market. Here, we show how perovskite solar modules, an emerging photovoltaic technology, can be fabricated in a scalable high-speed manner with improved power-conversion efficiency. The self-doping level in the perovskite materials is suppressed by a reduced annealing duration followed by room-temperature aging, leading to enhanced photovoltage output.

Yehao Deng, Zhenyi Ni, Axel F. Palmstrom, ..., Xun Xiao, Kai Zhu, Jinsong Huang

jhuang@unc.edu

HIGHLIGHTS

Perovskite solar module by scalable fabrication reached 17.8% aperture efficiency

Demonstrated a strategy to accelerate fabrication and improve efficiency simultaneously

Disclosed the correlations among annealing, self-doping, and efficiency in perovskite

Deng et al., Joule 4, 1–12
September 16, 2020
https://doi.org/10.1016/j.joule.2020.07.003

Please cite this article in press as: Deng et al., Reduced Self-Doping of Perovskites Induced by Short Annealing for Efficient Solar Modules, Joule (2020), https://doi.org/10.1016/j.joule.2020.07.003

Joule

CellPress

Article

Reduced Self-Doping of Perovskites Induced by Short Annealing for Efficient Solar Modules

Yehao Deng,[1] Zhenyi Ni,[1] Axel F. Palmstrom,[2] Jingjing Zhao,[1] Shuang Xu,[1] Charles H. Van Brackle,[1] Xun Xiao,[1] Kai Zhu,[2] and Jinsong Huang[1,3,*]

SUMMARY

Controlling of doping in semiconducting light absorber can minimize the charge recombination and maximizing power output from solar cells; however, it is challenging for perovskites due to lack of controlled doping. Here, we report that a short post-annealing of less than 3 min for facilitating high-throughput manufacturing of perovskite solar modules in an ambient environment maintains the stoichiometric composition of perovskites, encouraging a spontaneous de-doping of perovskites during aging. The reduced self-doping results in less charge recombination and, thus, higher device efficiency. The stabilized open-circuit voltage of sub-cells in the $CH_3NH_3PbI_3$ minimodules with an area >20 cm^2 reaches 1.19 V on average. The aperture efficiency reaches 17.8% under one sun and 18.7% under a quarter sun illumination, deriving an averaged efficiency >20.0% for each sub-cell with an area >3 cm^2, demonstrating the excellent uniformity of the films by this scalable process. The minimodule also works as uniform light-emitting devices.

INTRODUCTION

The efficiencies of lab-scale small-area perovskite solar cells have already exceeded 25%, which gives an unprecedented opportunity to scale up the fabrication of perovskite modules in industrial environment.[1–3] The low-cost perspective of perovskite solar cell technologies greatly leverages on the low-cost solution fabrication processes in addition to the low-cost raw materials, because of their low temperature and high throughput by a continuous process such as roll-to-roll fabrication. High-throughput continuous fabrication of perovskite solar modules demands not only high-speed deposition of perovskite and charge-transport-material thin films but also fast post-treatments on those films. The speed of perovskite deposition by the blading process has been increased to close 500 mm/s by us using recently developed ink formulation engineering.[4] What follows film deposition is the annealing process. Among all active layers of perovskite solar cells, the perovskite layer needs the longest annealing to dry the solution and grow the crystals. In the most reported fabrication process, long annealing from tens of minutes to hours are generally used to achieve the highest efficiency perovskite solar cells in labs to date.[5–8] However, this long annealing would impose significant challenges to perovskite solar panel manufacturing. For instance, fast perovskite blading process can produce 30-m-long perovskite films at a high speed of 500 mm/s, thus the oven will be > 500 m long to match the speed of blading if annealing takes >20 min.[5,7] This is clearly impractical due to the huge capital expense for equipment, energy input, footprint, and labor to maintain them.[9,10] In order to maintain the rapid

Context & Scale

Photovoltaics are reforming the energy structure globally. Perovskite solar cells, as an emerging photovoltaic technology, show great potential due to their high solar-to-electric power-conversion efficiency and solution processability. However, before it can enter the market and compete with traditional photovoltaic technologies, including silicon, cadmium telluride, and copper indium gallium selenide, perovskite solar cells need to realize scalable fabrication, cost effectiveness, and high performance (high efficiency and stability) simultaneously. This paper demonstrates a strategy to achieve improved performance and reduced cost in a scalable fabrication process by taking advantage of one of the features of perovskite materials—the self-doping or de-doping processes in the material. It can be one promising development direction for perovskite photovoltaics commercialization.

deposition of perovskites without adding additional annealing lines, the annealing time must be reduced. In addition, shortening the annealing duration saves energy consumption and accelerate the production.[11–15]

Here, we report the discovery that reducing the annealing time of perovskite films blade coated in fully ambient conditions can also improve the module efficiency. Comparing to a longer annealing, a short annealing of ~2.5 min in ambient condition produces perovskite films with more stoichiometric composition, which promotes a spontaneous de-doping process after fabrication that leads to more intrinsic perovskite films. The de-doping process proceeds in either bare films or completed devices after fabrication. We show that the resultant more intrinsic perovskite with reduced background carrier concentration leads to a slower recombination rate and then improved photovoltage and efficiency of p-i-n structured perovskite cells and modules without compromising stability. The same phenomenon was observed in perovskite materials and solar cells with different compositions with formamidinium (FA) and cesium (Cs), indicating the universal applicability of this approach to produce more efficient perovskite solar modules.

RESULTS AND DISCUSSION

The perovskite solar cells have a structure of glass/indium tin oxide (ITO)/ Poly[bis(4-phenyl)(2,4,6-trimethylphenyl)amine] (PTAA)/ $CH_3NH_3PbI_3$ ($MAPbI_3$)/ C_{60}/ Bathocuproine (BCP)/ Copper (Cu). The PTAA and perovskite layers were deposited on glass/ITO substrate by blade coating as developed by us previously, while the other layers were formed by thermal evaporation.[4] Here, the annealing condition for perovskite was 3 min at 100°C. We also annealed some perovskite films for 20 min at the same temperature as control samples. It is noted that annealing duration below 3 min would lead to less-reproducible device performances. A typical fabricated perovskite solar module with an aperture area of 21.5 cm^2 and 6 sub-cells is shown in Figure 1A. The current-voltage (*I-V*) scanning curves of a small-area single cell (0.08 cm^2) and a minimodule (21.5 cm^2) by the short annealing (3 min, 100°C) process under simulated AM1.5 illumination are shown in Figure 1B. With a perovskite band gap (E_g) of 1.55 V for $MAPbI_3$ as determined by the external quantum efficiency (shown in Figure S1), the stabilized open-circuit voltage (V_{OC}) of the single cell under one sun illumination reached 1.22 V (Figure 1C), leading to a small V_{OC} deficit of 0.33 V, which is among the lowest realized in perovskite solar cells reported.[6,16,17] When this short annealing method is applied to blade-coated minimodules, the V_{OC} deficit only slightly increased to 0.36 V with a mean stabilized sub-cell V_{OC} of 1.19 V (dividing the total V_{OC} of the minimodule by the number of sub-cells). The low V_{OC} deficit contributes to a stabilized aperture area (21.5 cm^2) efficiency of 17.8% (Figure 1D), which is the highest for perovskite minimodules published in the literature.[18,19] The efficiencies determined from forward and reverse *J-V* scanning curves of the minimodule are 17.7% and 18.0%, respectively, showing only a very small hysteresis (shown in Figure S2). We fabricated 11 minimodules, and the performance distribution is shown in Figure S3. Ten of 11 modules showed a mean V_{OC} of >1.16 V, and eight of them showed efficiencies of >17.0%, showing high reproducibility by this method. The minimodules performed even better under lower light intensity. Under a quarter sun intensity (25 mW/cm^2), the aperture efficiency of the minimodule increased to 18.7% (Figure 1E), which may be ascribed to the less resistive loss from ITO electrode as a result of smaller photocurrent. The V_{OC} and short circuit current variations under different light intensities are presented in Figure S4. The high photovoltages of the short-annealed devices are stable during long-term operation under continuous one sun illumination. As is shown

[1]Department of Applied Physical Sciences, University of North Carolina at Chapel Hill, Chapel Hill, NC 27599, USA

[2]National Renewable Energy Laboratory, Golden, CO 80401, USA

[3]Lead Contact

*Correspondence: jhuang@unc.edu

https://doi.org/10.1016/j.joule.2020.07.003

Please cite this article in press as: Deng et al., Reduced Self-Doping of Perovskites Induced by Short Annealing for Efficient Solar Modules, Joule (2020), https://doi.org/10.1016/j.joule.2020.07.003

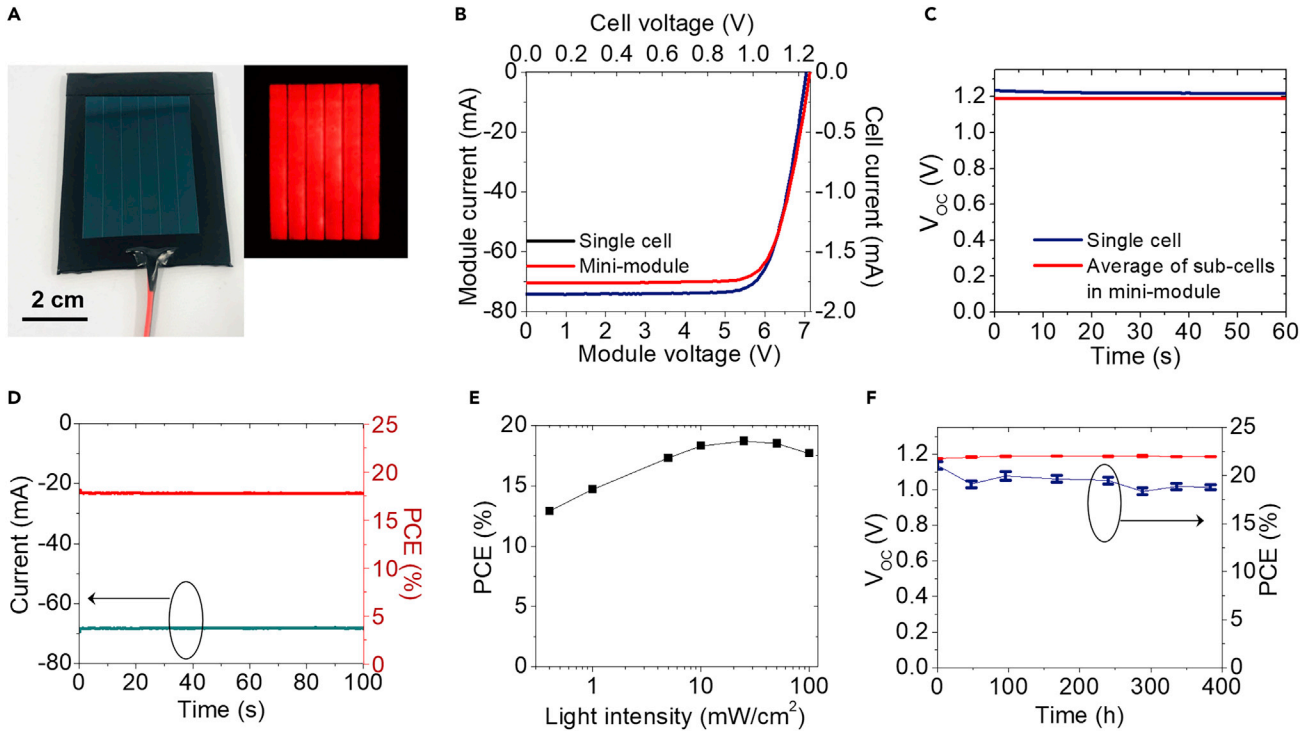

Figure 1. Performances of Perovskite Devices by Short Annealing

(A) Photo of a minimodule and its electroluminescence in dark captured by an IR responsive camera under a forward bias of 12 V.

(B and C) (B) The *I-V* scanning and (C) the stabilized V_{OC} of a small cell (8 mm^2) and a minimodule (21.5 cm^2) under one sun illumination.

(D) The stabilized photocurrent output of the minimodule under maximum powerpoint.

(E) The efficiency of a minimodule under different illumination intensity.

(F) Long-term stability of the photovoltage and power-conversion efficiency of perovskite devices under operating conditions.

in Figure 1F, their V_{OC} remained 100% of the initial value after 400 h of working near maximum power point (Figure 1F) and their efficiencies retained 90% of the initial values.

The geometrical filling factor (the ratio of the active area to the total aperture area) of the minimodules is 93.0%, and each sub-cell has an area of 3.32 cm^2. Therefore, the sub-cell efficiency reached 19.1% and 20.1% on average under one sun and a quarter sun illumination, respectively. Considering this efficiency is approaching that one can achieve in small-area devices, the distribution of sub-cell efficiencies in the minimodule should be very narrow, indicating an excellent uniformity of the perovskite films and other layers. Electroluminescence is a direct way to examine the uniformity of a large area solar module.[20] Under a forward bias of 12.0 V the minimodule delivered bright photoemission from the entire active area without obvious defective region (Figure 1A), which again demonstrates the excellent uniformity of the perovskite films.

The high photovoltage of the short-annealed devices comes from an aging process after device fabrication. The V_{OC} of the device annealed for 3 min under one sun illumination was initially 1.14 V right after device fabrication and then increased to 1.20 V after aging in the dark for 20 days (Figure 2A). We varied the light intensity from 100 to 4 mW/cm^2 and observed that the V_{OC} under all different light intensities increase by ~60 mV after aging (Figure 2A). In contrast, although the device annealed for 20 min was initially more efficient, its V_{OC} slightly decreased from 1.14

Please cite this article in press as: Deng et al., Reduced Self-Doping of Perovskites Induced by Short Annealing for Efficient Solar Modules, Joule (2020), https://doi.org/10.1016/j.joule.2020.07.003

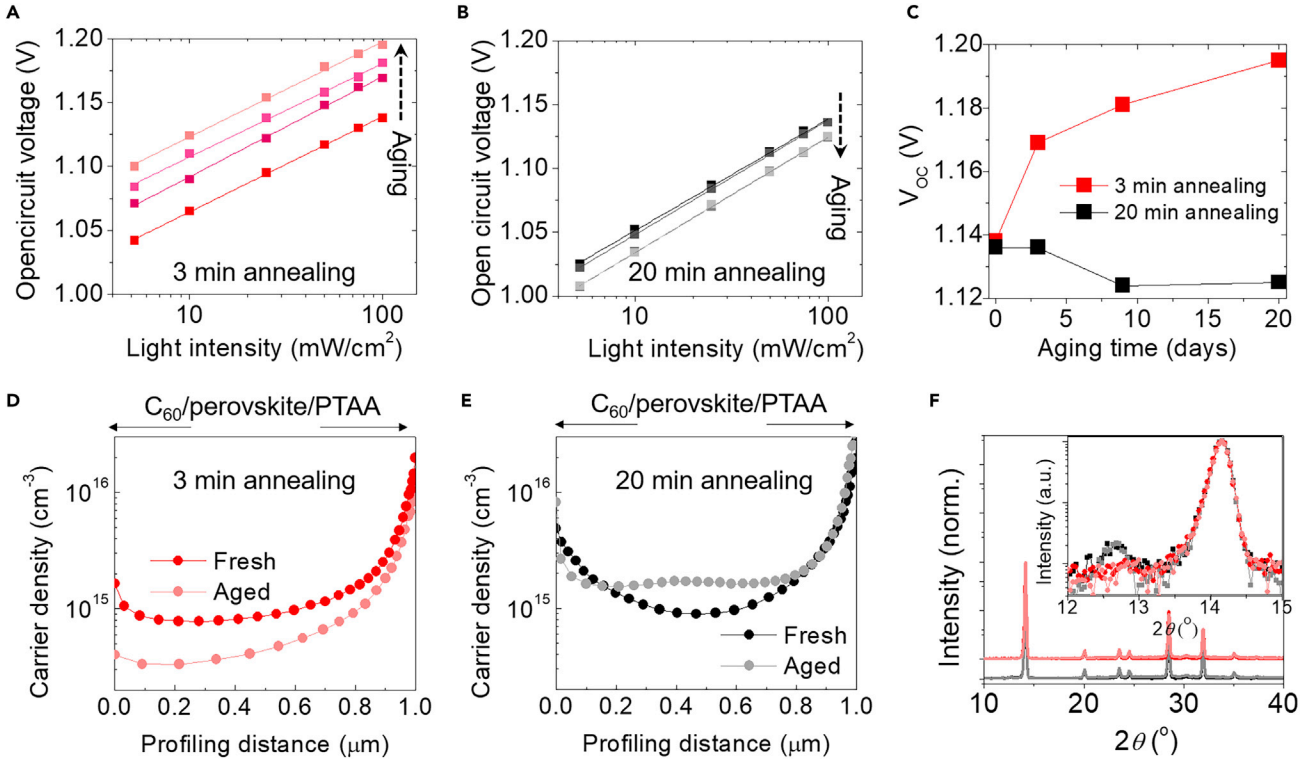

Figure 2. The De-doping Process in Perovskite Devices by Short Annealing

(A and B) The V_{OC} of devices as a function of illumination intensity with perovskite films annealed for (A) 3 and (B) 20 min during an aging period of 0, 3, 9, and 20 days.

(C) The evolution of V_{OC} of both devices under one sun illumination as a function of aging time in the dark.

(D and E) The distribution of free carriers in perovskite layer annealed for (D) 3 and (E) 20 min obtained by DLCP at 2 MHz before and after aging.

(F) XRD of perovskites annealed for 3 and 20 min before and after aging. Inset: amplified low angle region from 12.0° to 15°.

to 1.13 V after aging for 20 days with no improvement in efficiency (Figures 2B and S5). Figure 2C summarizes the evolution of V_{OC} measured under one sun illumination for both devices during 20 days of storage in dark.

We examined the possible differences between the two types of films annealed for 3 and 20 min before and after aging. First of all, it is noted that an annealing duration of 3 min at 100°C is long enough to remove the solvents from the films because no signal of the solvents was detected in the films by Fourier-transform infrared spectroscopy (FTIR) (Figure S6). Besides, we did not observe an obvious change of the perovskite film morphology or grain size during aging for both types of films, as shown by the top-view scanning electron microscopy images in Figure S7. Third, there was no significant change of deep trap density of states (tDOS) with an energy depth of approximately 0.25–0.55 V inside the band gap for both types of devices before and after aging, as measured by the thermal admittance spectroscopy (TAS) shown in Figure S8. In the region of 0.3–0.55 V, both types of devices show only a minor reduction of deep trap density by less than 20%. One difference between the two samples is that the film annealed for 3 min show pure perovskite phase derived from X-ray diffraction (XRD) patterns before and after aging, but the film annealed for 20 min contains a small amount of lead iodide phase with a new XRD peak at 12.6° (Figure 2F). The excessive lead iodide should be caused by the sublimation of volatile species during the longer annealing process. This is not easily avoided, especially when annealing needs to be conducted in the

Please cite this article in press as: Deng et al., Reduced Self-Doping of Perovskites Induced by Short Annealing for Efficient Solar Modules, Joule (2020), https://doi.org/10.1016/j.joule.2020.07.003

air with less controlled humidity for scalable fabrication in an industrial environment.[21,22] It has been reported that lead iodide-rich $MAPbI_3$ is n-type self-doped,[23] and this might be due to the generation of iodide vacancies (V_I) that act as electron donors with transition energies less than 0.05 eV below the conduction band.[24] We conducted the Hall effect measurement that confirmed that the films made by this method were n-type doped. To characterize the spatial distribution of doping in the real devices, we conducted drive-level capacitance profiling (DLCP) at a frequency of 2 MHz for both types of devices before and after aging. DLCP is recently shown to be an effective technique to characterize the spatial distribution of doping and charge traps with different depth in perovskite thin films and single crystals.[25] Measuring at a low frequency (e.g., <100 kHz) probes both trapped charges and doping, while measuring at a high frequency (e.g., 2 MHz or higher) can only detect those charges that are free to move either due to doping or thermally excited from very shallow traps. Here, by measuring the devices at 2 MHz in the dark, we observed that for the perovskite film annealed for 3 min, its free carrier concentration (i.e., doping concentration) decreased by up to one order of magnitude during aging for 20 days, especially in the region closer to the C_{60}/perovskite interface (Figure 2D). On the contrary, the free carrier concentration in the perovskite annealed for 20 min increases slightly in the central region of the film during the 20 days of aging (Figure 2E). We also measured the DLCP at a lower frequency range of 10 to 100 kHz to obtain the deep trap concentration. Consistent with the tDOS results by TAS measurement, there is no obvious change between the two types of films, shown in Figure S9. The trap density for both types of films slightly reduced by <30% during the 20 days of aging at locations across the film except those close to perovskite-PTAA interface. Our recent study has shown that the region close to the perovskite/PTAA interface is where most deep traps reside due to the presence of large density of nanocrystals and amorphous phase,[25] and the result shown here indicates aging itself is not effective in removing these extended structural defects.

The de-doping of perovskites after aging should impact the overall device efficiency. To better understand its impact, we simulated the device performance and energy band diagram in the cases of low and high doping levels in perovskite using solar cell capacitance simulator (SCAPS).[26] The doping profile in perovskites was constructed to follow the measured results by DLCP and the doping was set to be n-type. First, we simulated the energy band diagrams for both types of devices in the dark. The more intrinsic perovskite leads to a band tilting across the entire perovskite thickness (Figure 3A), while perovskite with a higher doping level leads to a band bending closer to the perovskite-HTL interface (Figure 3B). Then, we simulated the devices under one sun illumination condition. The more intrinsic perovskite has a V_{OC} of 1.20 V, while the one with a higher doping level has a V_{OC} of 1.14 V, agreeing well with the experimental results (Figure 3C). We further observed that the V_{OC} difference mainly comes from the different quasi-Fermi level splitting values, which are simulated to be 1.20 and 1.14 V under one sun illumination, respectively (Figures 3D and 3E). It also shows that in these p-i-n $MAPbI_3$ devices when the charge-transport layers have been well optimized with matched energy levels and strong charge extraction capability, the V_{OC} is determined by the quasi-Fermi level splitting in the $MAPbI_3$ layer.[27] Under one-sun illumination, the photo-generated carrier concentrations in the perovskite layers are on the order of 10^{15}–10^{16} cm^{-3},[28] which is within the same range with the measured doping concentration in the perovskite films annealed for 20 min. The higher background charge concentration may lead to increased charge recombine with the photo-generated charge carriers, thus reducing the population of photo-generated carriers and decreasing quasi-Fermi level splitting. We simulated the recombination rate across the perovskite layer in

Please cite this article in press as: Deng et al., Reduced Self-Doping of Perovskites Induced by Short Annealing for Efficient Solar Modules, Joule (2020), https://doi.org/10.1016/j.joule.2020.07.003

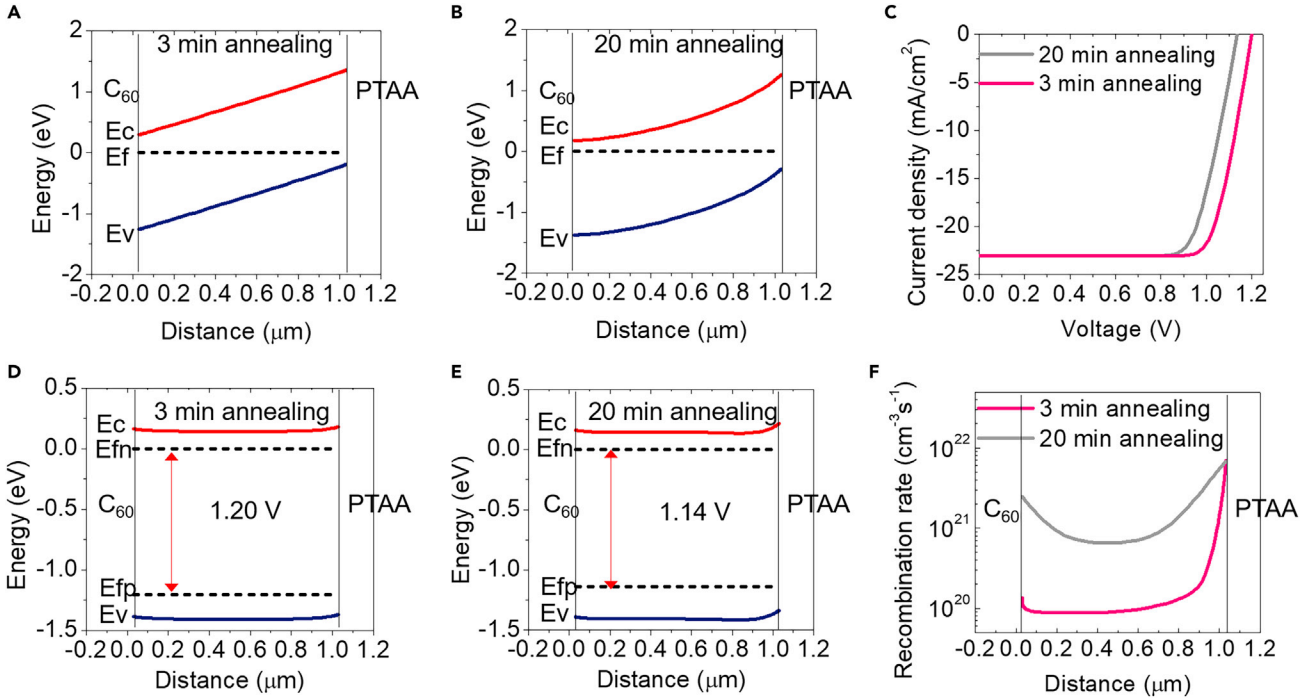

Figure 3. SCAPS Device Simulations of Perovskite by Different Annealing Durations

(A and B)Simulated energy band diagrams of devices in dark with perovskite layer annealed for (A) 3 and (B) 20 min. The Fermi level of the electron is set to be at 0 eV.

(C) Simulated J-V curves of the devices.

(D and E) Energy band diagrams of devices under one sun illumination with perovskite layer annealed for (D) 3 and (E) 20 min.

(F) Recombination rate distribution in the devices under one sun illumination and 1.14 V bias.

both types of devices under one sun illumination under 1.14 V. For both type of devices, the charge recombination rates in the regions close to charge-transport layers are higher than that in the interior (Figure 3F) due to higher doping concentrations in those regions (Figures 2D and 2E). Nevertheless, the device with more intrinsic perovskite exhibited smaller recombination rate by up to one order of magnitude than the one with a higher doping level. The latter has an integrated total recombination rate of 1.5×10^{17} $cm^{-2}s^{-1}$, while the former has a lower value of 2.3×10^{16} $cm^{-2}s^{-1}$, showing that its photo-generated carrier concentration can increase further until the recombination rate reaches the generation rate, allowing a larger quasi-fermi-level splitting and, thus, photovoltage output.

The aging-induced de-doping occurs not only in completed devices but also in bare films. The photoluminescence (PL) intensity of the bare film deposited on glass and annealed for 3 min increased by 322% at the peak wavelength during storage in N_2 filled glovebox for 20 days with its peak blue-shifted from 769 to 766 nm (Figure S10A), indicating a reduced defect concentration.[29] In the meantime, we observed a slightly improved crystallinity of the film during aging, as shown by the reduced full width at half maximum (FWHM) of the (110) XRD peak from 0.23° to 0.21° (Figure S10C). In contrast, the PL intensity of the film annealed for 20 min remained almost unchanged during the same aging period and its peak stayed around 772 nm (Figure S10A). The FWHM of its (110) XRD peak remained to be 0.23° (Figure S10D), showing no improvement in crystallinity. We performed photothermal deflection spectroscopy measurements on both types of perovskite films on quartz substrates after aging (Figure S10B). The results

Please cite this article in press as: Deng et al., Reduced Self-Doping of Perovskites Induced by Short Annealing for Efficient Solar Modules, Joule (2020), https://doi.org/10.1016/j.joule.2020.07.003

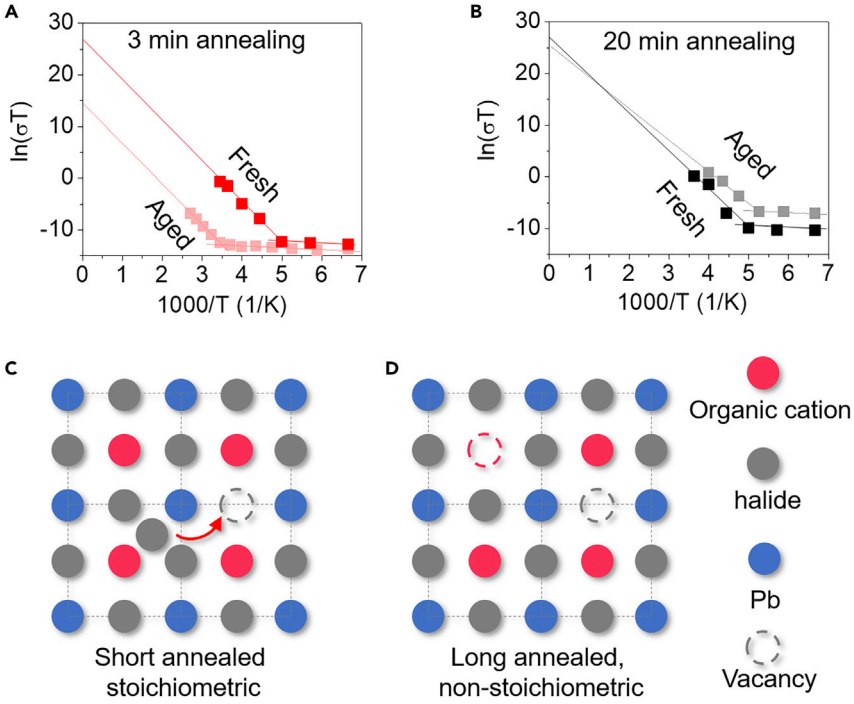

Figure 4. Ion Migration in Perovskite Films by Different Annealing Durations

(A and B) Ion migration characterizations for perovskite films annealed for (A) 3 and (B) 20 min annealing before and after aging as a function of temperature.

(C and D) Schematic illustration of the transition in perovskite materials annealed for (C) 3 and (D) 20 min during aging.

confirmed that the one annealed for 3 min had a smaller defect density of states with energies within 0.05 eV below the band gap.

To further understand the origin of reduced doping in the perovskite films during the aging process, we studied the variation of structural defect density in perovskite films by characterizing the ion migration in the films before and after aging by measuring the films' conductivity at different temperatures. The measured transition temperature, at which ion migration starts to dominate the total conductivity, can reflect the structural defect density, particularly iodide vacancies due to its fastest migration capability because ion migration occurs through structural defects. The relationship between temperature (T) and ionic conductivity (σ) is given as:

$$ln(\sigma T) = ln\sigma_0 - E_a^{eff}\frac{1}{kT} \quad \text{(Equation 1)}$$

$$\sigma_0 = \frac{Z_i e^2 C_v D}{k} \quad \text{(Equation 2)}$$

where E_a^{eff} is the activation energy for ions, Z_i is the valence of the ions, e is the elementary charge, C_v is vacancy concentration for ion migration, D is the diffusion coefficient.[30,31] By plotting $ln(\sigma T)$ as a function of $1{,}000/(T)$ we can get the information of E_a^{eff} and σ_0, which are represented by the slope of the fitting line and intercept of the fitting line with y axis, respectively. First of all, at low temperatures, ions are immobilized so that free carriers dominate the electrical conductivity with a small E_a^{eff} as shown by small slopes (Figures 4A and 4B). The E_a^{eff} fall in the range of 23–28 meV, proving that the shallow defects at these energy levels act as dopants

Please cite this article in press as: Deng et al., Reduced Self-Doping of Perovskites Induced by Short Annealing for Efficient Solar Modules, Joule (2020), https://doi.org/10.1016/j.joule.2020.07.003

that increase the free carrier concentration in the perovskite films. As temperature increases to a critical value or defined as the transition temperature, ion migration induced current starts to dominate the total conduction. The energy barrier is much larger for the migration of ions, shown by the much larger slope of the fitting line, or E_a^{eff}. We observed that the transition temperature for the film annealed for 3 min increased from ~200 to ~290 K during aging (Figure 4A), accompanied with a decreased intercept value, or σ_0, and thus a decreased vacancy concentration C_v. In the meantime, the E_a^{eff} increased slightly from 0.651 to 0.666 eV. In contrast, the σ_0 for the film annealed for 20 min stayed almost unchanged, and its E_a^{eff} decreased from 0.672 to 0.519 eV (Figure 4B).

The results prove that the structure-defect density changes induced by aging are different for the two types of samples, which can be explained by their material structure and/or composition difference at the initial stage of aging. The conversion of perovskite solution into polycrystalline perovskite films in the blading process involves multiple steps of solvent evaporation, intermediate phase formation and decomposition, grain nucleation and growth, etc. Unlike single crystal growth, which takes much longer time to grow, the formation of solid-state phases in bladed perovskite films occurs quickly within seconds, and thus it is highly likely that there are many ions that do not reside at the lattice positions. The large density of structural defects increases the contribution from ion migration to total conductivity, explaining the observation shown in Figures 4A and 4B. In defective films, not only more ions can move, but also ions move faster according to ion diffusion theory.[32] Some structural defects such as iodide vacancies have been reported to induce self-doping in perovskites.[24] An annealing may help these ions to return to their lattice position by accelerating ion diffusion rate; however, too long annealing also causes the evaporation of volatile species such as the organic cations and iodide anions from perovskite films, making them less stoichiometric. This is evidenced by the observation of PbI_2 in the $MAPbI_3$ films annealed for 20 min in this work and many others.[15,33,34] Aging process can self-repair some misfit defects, but the non-stoichiometry induced defects cannot be eliminated, unless there are more precursor ions can be added into the films again. On the contrary, the film annealed for a short duration of ~2.5 min retained the stoichiometric composition. Although there was still a high density of misfit defects in these films right after annealing, evidenced by the high doping in these films, ion diffusion at room temperature can eliminate most of the misfit defects as long as enough time is given, which eventually results in de-doping of the perovskites.

To investigate whether the short annealing approach is generally applicable to perovskites with other compositions, we bladed MA-free perovskite films based on FA and Cs cations, which are reported to be more thermally stable than $MAPbI_3$.[35] The detailed fabrication process for a composition of $FA_{0.92}Cs_{0.08}PbI_3$ is described in the method section of Supplemental Information. We observed that a short annealing of 2 min at 150°C leads to a perovskite solar cell with an initial efficiency of 18.0%, which then spontaneously increased to 20.3% after aging for 11 days (Figure S11A). Again, DLCP profiling showed that the carrier density decreased by up to 10 times in the region closer to the C_{60}-perovskite interface (Figure S11C). It indicates the same spontaneous defect annihilation process makes the $FA_{0.92}Cs_{0.08}PbI_3$ films to be more intrinsic. However, though a slightly longer annealing of 10 min at the same temperature results in an initial efficiency of 17.9%, the efficiency improvement during aging is much smaller (Figure S11B). Only a slight reduction in carrier density in the central region of the perovskite film by less than 40% is observed (Figure S11D). The result indicates that shorting the annealing duration in air is still beneficial for FA-

Please cite this article in press as: Deng et al., Reduced Self-Doping of Perovskites Induced by Short Annealing for Efficient Solar Modules, Joule (2020), https://doi.org/10.1016/j.joule.2020.07.003

Cs-based perovskites for reduced self-doping. Last, it should be noted that to the perovskite films we have added chlorine (Cl^-) ions as one of the additives. It is possible that shorter annealing allows more Cl^- residue in the films, which tend to fill the iodine vacancies during aging, while the other additives might be too large to affect the doping/de-doping of perovskites because they cannot get into the lattice position.

In summary, this work highlights the effects of a short annealing process to obtain more intrinsic perovskite films by scalable fabrication in an ambient environment for higher efficiencies in perovskite devices. The short annealing treatment maintains the stoichiometric composition of perovskite and allows a notable spontaneous de-doping process, which is absent in perovskite films treated by conventional long annealing. This work proposed a strategy for reducing module fabrication costs and improving module performance simultaneously in industrial fabrication. Since the spontaneous de-doping process can happen in completed devices, the commercialized solar modules can take advantage of storage and shipping periods to reach maximum efficiency without sacrificing the manufacturing throughput.

EXPERIMENTAL PROCEDURES

Resource Availability

Lead Contact

Further information and requests for resources and materials should be directed to and will be fulfilled by the Lead Contact, Jinsong Huang (jhuang@unc.edu).

Materials Availability

This study did not generate new unique materials.

Data and Code Availability

The data presented in this work are available from the corresponding authors upon reasonable request.

Materials

All chemicals were purchased from Sigma Aldrich unless otherwise specified and used without further purification. Methylammonium hypophosphite was synthesized according to our previous publication (Energy & Environmental Science, 2016, 9(3): 867–872). Methylammonium iodide was purchased from Greatcell Solar. C_{60} is purchased from Nano-C. Copper for thermal evaporation is obtained from Kurt J. Lesker company.

Device Fabrication

ITO-glass substrates for small-area single cells were washed with isopropanol and acetone sequentially and dried in an oven at 60°C. PTAA dissolved in toluene was blade coated on UV-ozone treated ITO/glass substrate at 20 mm/s with 200 μm coating gap. Then the $MAPbI_3$ perovskite layer was blade coated per to our recently developed room-temperature blade-coating method (Science advances, 2019, 5(12): eaax7537). L-α-Phosphatidylcholine, methylammonium chloride, methylammonium hypophosphite, and phenylethyl ammonium chloride were added into the solution as additives at molar percentages of ~0.025%, ~0.8%, ~1.0%, and ~0.15% to $MAPbI_3$, respectively. The as-coated solid film was annealed at 100°C in air for 3 or 20 min. The $FA_{0.92}Cs_{0.08}PbI_3$ perovskite films were also blade coated at room temperature under nitrogen knife blowing by using a precursor solution containing 1.0 M $FAPbI_3$ and 0.09 M $CsPbI_3$ dissolved in a 2-methoxyethanol:dimethyl sulfoxide solvent mixture. Formamidinium chloride and phenylethyl

Please cite this article in press as: Deng et al., Reduced Self-Doping of Perovskites Induced by Short Annealing for Efficient Solar Modules, Joule (2020), https://doi.org/10.1016/j.joule.2020.07.003

ammonium chloride were added into the solution as additives at molar percentages of ~1.5% and ~0.15% to Pb^{2+} ions, respectively. The as-coated solid film was annealed at 150°C in air for 2 or 10 min. Then the perovskite films were thermal evaporated with C_{60} (30 nm), BCP (6 nm), and copper (80 nm) to complete the device fabrication. For fabricating modules, pre-patterned ITO substrates were used. Laser ablation was applied before and after the deposition of the metal electrode to complete the series interconnection between sub-cells in the module.

Material and Device Characterizations

Unless specified, all device tests were conducted in air at ambient temperatures. The *J-V* scanning of perovskite single cells and modules were done with a Keithley 2400 Source-Meter under simulated solar illumination produced by a Xenon-lamp-based solar simulator (Oriel Sol3A, Class AAA Solar Simulator) under different light intensities. The light intensity was calibrated by a certified silicon reference cell (Newport 91150V-KG5). The modules were masked with black tape and the area of the rectangular-shaped apertures were determined before testing. The scan rate was 0.2 V/s for small-area single cells and 1 V/s for modules. There was no preconditioning before measurement. The external quantum efficiency of the module was obtained with a Newport QE measurement kit. The integrated photocurrent is 21.9 mA/cm^2, which agrees with the value of module measured from *J-V* scanning (21.2 mA/cm^2). To measure the long-term operational stability of perovskite devices, three devices were encapsulated, illuminated by one sun equivalent metal halide lamp without UV filter, and connected with resistors that maintain the devices to work near the maximum power points. The devices worked at temperatures of about ~35°C. The V_{OC} change of the devices during operation were recorded repetitively by removing the resistors and reading the stabilized values under one sun illumination and the efficiencies were obtained by performing *J-V* scanning. The TAS and DLCP were measured by an E4980A Precision LCR Meter from Agilent. The photoluminescence spectra of perovskite films were obtained with a Horiba DeltaPro time-correlated single-photon counting (TCSPC) fluorometer. The ion migration activation energies of perovskite films were measured with a temperature controllable probe station. The FTIR spectra were collected in the transmittance mode on a PerkinElmer IR spectrometer. The scanning electron microscopy (SEM) images were taken by a Quanta 200 FEG environmental scanning electron microscope. The XRD pattern was obtained with a Rigaku sixth generation MiniFlex X-ray diffractometer. Photothermal deflection spectroscopy (PDS) measurements were carried out using a home-made system, which is equipped with a 100-W halogen lamp and a three-grating monochromator. Perovskite samples were immersed in Fluorinert FC-3283 (3M), whose refractive index changes with temperature to provide a thermal signal from the samples. Monochromatic excitation light is focused through an aperture on the sample surface and a He-Ne laser is aligned parallel to the sample surface. Localized heating due to monochromatic photon absorption leads to deflection of the laser, which is detected using an (A-B) silicon diode position detector and a lock-in amplifier (Stanford SR810).

Device Simulations

The device simulations were performed with the SCAPS software developed by the University of Gent, Belgium. A basic planar p-i-n structure of hole transporting layer (HTL)-perovskite-electron transporting layer (ETL) was constructed for the solar cell simulations. To perform the comparative study between the 3 and 20 min annealed perovskite, all parameters were set to be identical in the simulations except the energy and spatial distribution of shallow defects in perovskite. The shallow defects are set to be electron donors with energy levels centered at 0.01–0.03 eV below the

conduction band with gaussian distributions of 0.02–0.04 eV. Their spatial distributions were constructed with beta functions to resemble the measured results in the 3 and 20 min annealed perovskite films respectively as were obtained by DLCP in Figure 2.

The detailed simulation parameters are shown in the Table S1 in the Supplemental Information.

SUPPLEMENTAL INFORMATION

Supplemental Information can be found online at https://doi.org/10.1016/j.joule.2020.07.003.

ACKNOWLEDGMENTS

This work was supported by Office of Naval Research under awards N00014-17-1-2619, U.S. Department of Energy's Office of Energy Efficiency and Renewable Energy (EERE) under Solar Energy Technologies Office (SETO) agreement number DE-EE0008749, and University of North Carolina's Research Opportunities Initiative (UNC ROI) through Center of Hybrid Materials Enabled Electronic Technology. We also thank the financial support from the Center for Hybrid Organic Inorganic Semiconductors for Energy (CHOISE), an Energy Frontier Research Center funded by the DOE Office of Basic Energy Sciences, Office of Science. This work was performed in part at the Chapel Hill Analytical and Nanofabrication Laboratory, CHANL, a member of the North Carolina Research Triangle Nanotechnology Network, RTNN, supported by the National Science Foundation, grant ECCS-1542015, as part of the National nanotechnology Coordinated Infrastructure, NNCI. The work at the National Renewable Energy Laboratory was supported by the U.S. Department of Energy under contract no. DE-AC36-08GO28308 with Alliance for Sustainable Energy, Limited Liability Company (LLC), the Manager and Operator of the National Renewable Energy Laboratory. The views expressed in the article do not necessarily represent the views of the DOE or the U.S. Government. The U.S. Government retains and the publisher, by accepting the article for publication, acknowledges that the U.S. Government retains a nonexclusive, paid-up, irrevocable, worldwide license to publish or reproduce the published form of this work or allow others to do so, for U.S. Government purposes.

AUTHOR CONTRIBUTIONS

J.H., Y.D., and Z.N. conceived the idea and designed the experiments of this work. Y.D. fabricated and characterized the perovskite thin films and devices. Y.D. and Z.N. performed the device simulations. Z.N., Y.D., and S.X. conducted the DLCP measurements. Y.D. and C.H.V.B. did the PL tests. J.Z. and X.X. performed the XRD characterizations. A.F.P. and K.Z. conducted the PDS measurements. J.H. and Y.D. wrote the manuscript, and all the authors reviewed the manuscript.

DECLARATION OF INTERESTS

The authors declare no competing interests.

Received: May 22, 2020
Revised: June 14, 2020
Accepted: June 30, 2020
Published: July 29, 2020

Please cite this article in press as: Deng et al., Reduced Self-Doping of Perovskites Induced by Short Annealing for Efficient Solar Modules, Joule (2020), https://doi.org/10.1016/j.joule.2020.07.003

REFERENCES

1. Li, Z., Klein, T.R., Kim, D.H., Yang, M., Berry, J.J., van Hest, M.F.A.M., and Zhu, K. (2018). Scalable fabrication of perovskite solar cells. Nat. Rev. Mater. *3*, 18017.
2. Park, N.-G., and Zhu, K. (2020). Scalable fabrication and coating methods for perovskite solar cells and solar modules. Nat. Rev. Mater. *5*, 333–350.
3. NREL (2020). Best research-cell efficiency chart. https://www.nrel.gov/pv/cell-efficiency.html.
4. Deng, Y., Van Brackle, C.H., Dai, X., Zhao, J., Chen, B., and Huang, J. (2019). Tailoring solvent coordination for high-speed, room-temperature blading of perovskite photovoltaic films. Sci. Adv. *5*, eaax7537.
5. Bi, D., Li, X., Milić, J.V., Kubicki, D.J., Pellet, N., Luo, J., LaGrange, T., Mettraux, P., Emsley, L., Zakeeruddin, S.M., and Grätzel, M. (2018). Multifunctional molecular modulators for perovskite solar cells with over 20% efficiency and high operational stability. Nat. Commun. *9*, 4482.
6. Jiang, Q., Zhao, Y., Zhang, X., Yang, X., Chen, Y., Chu, Z., Ye, Q., Li, X., Yin, Z., and You, J. (2019). Surface passivation of perovskite film for efficient solar cells. Nat. Photonics *13*, 460–466.
7. Min, H., Kim, M., Lee, S.U., Kim, H., Kim, G., Choi, K., Lee, J.H., and Seok, S.I. (2019). Efficient, stable solar cells by using inherent bandgap of α-phase formamidinium lead iodide. Science *366*, 749–753.
8. Zheng, X., Hou, Y., Bao, C., Yin, J., Yuan, F., Huang, Z., Song, K., Liu, J., Troughton, J., Gasparini, N., et al. (2020). Managing grains and interfaces via ligand anchoring enables 22.3%-efficiency inverted perovskite solar cells. Nat. Energy *5*, 131–140.
9. Song, Z., McElvany, C.L., Phillips, A.B., Celik, I., Krantz, P.W., Watthage, S.C., Liyanage, G.K., Apul, D., and Heben, M.J. (2017). A technoeconomic analysis of perovskite solar module manufacturing with low-cost materials and techniques. Energy Environ. Sci. *10*, 1297–1305.
10. Cai, M., Wu, Y., Chen, H., Yang, X., Qiang, Y., and Han, L. (2017). Cost-performance analysis of perovskite solar modules. Adv. Sci. *4*, 1600269.
11. Troughton, J., Carnie, M.J., Davies, M.L., Charbonneau, C., Jewell, E.H., Worsley, D.A., and Watson, T.M. (2016). Photonic flash-annealing of lead halide perovskite solar cells in 1 ms. J. Mater. Chem. A *4*, 3471–3476.
12. Sanchez, S., Hua, X., Phung, N., Steiner, U., and Abate, A. (2018). Flash infrared annealing for antisolvent-free highly efficient perovskite solar cells. Adv. Energy Mater. *8*, 1702915.
13. Yang, M., Li, Z., Reese, M.O., Reid, O.G., Kim, D.H., Siol, S., Klein, T.R., Yan, Y., Berry, J.J., Van Hest, M.F.A.M., and Zhu, K. (2017). Perovskite ink with wide processing window for scalable high-efficiency solar cells. Nat. Energy *2*, 17038.
14. Troughton, J., Charbonneau, C., Carnie, M.J., Davies, M.L., Worsley, D.A., and Watson, T.M. (2015). Rapid processing of perovskite solar cells in under 2.5 seconds. J. Mater. Chem. A *3*, 9123–9127.
15. Pool, V.L., Dou, B., Van Campen, D.G., Klein-Stockert, T.R., Barnes, F.S., Shaheen, S.E., Ahmad, M.I., Van Hest, M.F., and Toney, M.F. (2017). Thermal engineering of $FAPbI_3$ perovskite material via radiative thermal annealing and in situ XRD. Nat. Commun. *8*, 14075.
16. Luo, D., Yang, W., Wang, Z., Sadhanala, A., Hu, Q., Su, R., Shivanna, R., Trindade, G.F., Watts, J.F., Xu, Z., et al. (2018). Enhanced photovoltage for inverted planar heterojunction perovskite solar cells. Science *360*, 1442–1446.
17. Yoo, J.J., Wieghold, S., Sponseller, M.C., Chua, M.R., Bertram, S.N., Hartono, N.T.P., Tresback, J.S., Hansen, E.C., Correa-Baena, J.-P., Bulović, V., et al. (2019). An interface stabilized perovskite solar cell with high stabilized efficiency and low voltage loss. Energy Environ. Sci. *12*, 2192–2199.
18. Bi, E., Tang, W., Chen, H., Wang, Y., Barbaud, J., Wu, T., Kong, W., Tu, P., Zhu, H., Zeng, X., et al. (2019). Efficient perovskite solar cell modules with high stability enabled by iodide diffusion barriers. Joule *3*, 2748–2760.
19. Jung, E.H., Jeon, N.J., Park, E.Y., Moon, C.S., Shin, T.J., Yang, T.Y., Noh, J.H., and Seo, J. (2019). Efficient, stable and scalable perovskite solar cells using poly (3-hexylthiophene). Nature *567*, 511–515.
20. Gerber, A., Huhn, V., Tran, T.M.H., Siegloch, M., Augarten, Y., Pieters, B.E., and Rau, U. (2015). Advanced large area characterization of thin-film solar modules by electroluminescence and thermography imaging techniques. Sol. Energy Mater. Sol. Cells *135*, 35–42.
21. Song, Z., Abate, A., Watthage, S.C., Liyanage, G.K., Phillips, A.B., Steiner, U., Graetzel, M., and Heben, M.J. (2016). Perovskite solar cell stability in humid air: partially reversible phase transitions in the PbI_2-CH_3NH_3I-H_2O system. Adv. Energy Mater. *6*, 1600846.
22. Dai, X., Deng, Y., Van Brackle, C.H., Chen, S., Rudd, P.N., Xiao, X., Lin, Y., Chen, B., and Huang, J. (2020). Scalable fabrication of efficient perovskite solar modules on flexible glass substrates. Adv. Energy Mater. *10*, 1903108.
23. Wang, Q., Shao, Y., Xie, H., Lyu, L., Liu, X., Gao, Y., and Huang, J. (2014). Qualifying composition dependent p and n self-doping in $CH_3NH_3PbI_3$. Appl. Phys. Lett. *105*, 163508.
24. Yin, W.-J., Shi, T., and Yan, Y. (2014). Unusual defect physics in $CH_3NH_3PbI_3$ perovskite solar cell absorber. Appl. Phys. Lett. *104*, 063903.
25. Ni, Z., Bao, C., Liu, Y., Jiang, Q., Wu, W.Q., Chen, S., Dai, X., Chen, B., Hartweg, B., Yu, Z., et al. (2020). Resolving spatial and energetic distributions of trap states in metal halide perovskite solar cells. Science *367*, 1352–1358.
26. Burgelman, M., Nollet, P., and Degrave, S. (2000). Modelling polycrystalline semiconductor solar cells. Thin Solid Films *361–362*, 527–532.
27. Guo, D., Caselli, V.M., Hutter, E.M., and Savenije, T.J. (2019). Comparing the calculated Fermi level splitting with the open-circuit voltage in various perovskite cells. ACS Energy Lett. *4*, 855–860.
28. Huang, J., Yuan, Y., Shao, Y., and Yan, Y. (2017). Understanding the physical properties of hybrid perovskites for photovoltaic applications. Nat. Rev. Mater. *2*, 17042.
29. Shao, Y., Xiao, Z., Bi, C., Yuan, Y., and Huang, J. (2014). Origin and elimination of photocurrent hysteresis by fullerene passivation in $CH_3NH_3PbI_3$ planar heterojunction solar cells. Nat. Commun. *5*, 5784.
30. Pan, W., Wu, H., Luo, J., Deng, Z., Ge, C., Chen, C., Jiang, X., Yin, W.-J., Niu, G., Zhu, L., et al. (2017). $Cs_2AgBiBr_6$ single-crystal X-ray detectors with a low detection limit. Nat. Photonics *11*, 726–732.
31. Xing, J., Wang, Q., Dong, Q., Yuan, Y., Fang, Y., and Huang, J. (2016). Ultrafast ion migration in hybrid perovskite polycrystalline thin films under light and suppression in single crystals. Phys. Chem. Chem. Phys. *18*, 30484–30490.
32. Balluffi, R.W., Allen, S.M., and Carter, W.C. (2005). Kinetics of Materials (John Wiley & Sons Press).
33. Chen, Q., Zhou, H., Song, T.B., Luo, S., Hong, Z., Duan, H.S., Dou, L., Liu, Y., and Yang, Y. (2014). Controllable self-induced passivation of hybrid lead iodide perovskites toward high performance solar cells. Nano Lett. *14*, 4158–4163.
34. Dou, B., Pool, V.L., Toney, M.F., and van Hest, M.F.A.M. (2017). Radiative thermal annealing/in situ x-ray diffraction study of methylammonium lead triiodide: effect of antisolvent, humidity, annealing temperature profile, and film substrates. Chem. Mater. *29*, 5931–5941.
35. Turren-Cruz, S.H., Hagfeldt, A., and Saliba, M. (2018). Methylammonium-free, high-performance, and stable perovskite solar cells on a planar architecture. Science *362*, 449–453.